

Dust in Starburst Galaxies

Karl D. Gordon

Ritter Astrophysical Research Center, The University of Toledo, Toledo, OH 43606

Daniela Calzetti

Space Telescope Science Institute, 3700 San Martin Dr., Baltimore, MD 21218

and

Adolf N. Witt

Ritter Astrophysical Research Center, The University of Toledo, Toledo, OH 43606

ABSTRACT

To investigate the nature of starbursts' dust, we constructed a model of the stars and dust in starburst galaxies and applied it to 30 observed starburst spectral energy distributions (SEDs). The starburst model was constructed by combining two stellar evolutionary synthesis models with a model describing the radiative transfer of stellar photons through dust. The stellar evolutionary synthesis models were used to compute the dust-free SEDs for stellar populations with ages between 1×10^6 and 15×10^9 years. Using a Monte Carlo radiative transfer model, the effects of dust were computed for average Milky Way (MW) and Small Magellanic Cloud (SMC) dust, two different star/dust geometries, and locally homogeneous or clumpy dust. Using color-color plots, the starburst model was used to interpret the behavior of 30 starbursts with aperture-matched UV and optical SEDs (and IR for 19 of the 30) from previous studies. From the color-color plots, it was evident that the dust in starbursts has an extinction curve lacking a 2175 Å bump, like the SMC curve, and a steep far-UV rise, intermediate between the MW and SMC curves. The star/dust geometry which is able to explain the distribution of the 30 starbursts in various color-color plots has an inner dust-free sphere of stars surrounded by an outer star-free shell of clumpy dust. When combined with other work from the literature on the Orion region and the 30 Dor region of the Large Magellanic Cloud, this work implies a trend in dust properties with star formation intensity.

Subject headings: dust, extinction — galaxies: ISM — galaxies: starburst — galaxies: stellar content — radiative transfer

1. Introduction

The intrinsic spectral energy distribution (SED) of a galaxy can tell us much about that galaxy's stellar evolutionary history, but dust affects the intrinsic SED in a complicated fashion. The effects of dust on a galaxy's SED are determined by the physical properties and spatial distribution of the dust. Our knowledge of the physical properties and spatial distribution of dust in galaxies other than the Milky Way (MW) and the Magellanic Clouds is very limited. Starburst galaxies are good objects in which to study dust as their energetic output is dominated by massive stars and they are bright in the ultraviolet (UV) where the effects of dust are large. In addition, proper removal of the dust's effects is necessary in order to study the starburst's stellar evolutionary history (i.e. age, star formation rate, initial mass function, etc.).

The physical properties of dust affecting a galaxy's SED are parameterized by the wavelength dependence of the dust's extinction, albedo, and scattering phase function. The extinction curve is the dominant physical property and the easiest to determine observationally. Extinction curves for stars in our Galaxy, the Small & Large Magellanic Clouds (SMC & LMC), and (tentatively) M31 have been determined and found to have a common shape, but exhibit significant variations. Generally, the extinction increases with decreasing wavelength, making the effects of dust strongest in the UV. The most prominent feature in UV/optical extinction curves is the 2175 Å bump, which varies greatly in strength in our Galaxy (Witt, Bohlin, & Stecher 1984; Cardelli, Clayton, & Mathis 1989) and the LMC (Fitzpatrick 1985), is absent in the SMC (Prévot et al. 1984, but see Lequeux et al. 1982 for an exception), and seems weaker in M31 than in our Galaxy (Bianchi et al. 1996). The behavior of the 2175 Å bump in the LMC seems particularly relevant to the question of the type of dust present in starbursts. The average extinction curve for the 30 Dor region shows a very weak 2175 Å bump and a strong far-UV rise, while the average extinction curve for stars outside the 30 Dor region shows a 2175 Å bump strength and far-UV rise comparable to that of the average Galactic 2175 Å bump (Clayton & Martin 1985; Fitzpatrick 1985; Fitzpatrick 1986). This behavior implies the extinction curve in starbursts may be more like the extinction in the 30 Dor region, lacking a significant 2175 Å bump and having a strong far-UV rise. In fact, the 30 Dor region has

been described as the Rosetta Stone for starbursts as it is the most massive star cluster in the Local Group (Hunter et al. 1995) and it is close enough to study individual stars (Walborn 1991).

The spatial distribution of the dust plays a crucial role in determining the strength of dust's effects on the SED of a galaxy. Witt, Thronson, & Capuano (1992, hereafter WTC) investigated the effects of different spherical distributions of dust and stars (termed galactic environments) using a Monte Carlo radiative transfer model. Their finding was that the SED of a galaxy will always be dominated by the least attenuated stars as they contribute the most flux to the SED. As a result, the signatures of dust seen in the galaxy SED will almost always imply small amounts of dust. Recently, Witt & Gordon (1996) studied the radiative transfer in a clumpy (two-phase) dust distribution. They found the clumpiness resulted in more photons escaping than in the equivalent homogeneous case as the inter-clump medium provides small optical depth paths. The dust in galaxies is distributed in clouds (e.g. Dickey & Garwood 1989; Scalo 1990; Rosen & Bregman 1995), implying clumpiness is necessary to include in any radiative transfer model involving dust in galaxies.

In discussing the effects of dust in galaxies, it is important to distinguish between a galaxy's attenuation curve and the dust's extinction curve in that galaxy. The dust's extinction curve is directly related to the physical properties of the dust grains. An extinction curve can be observationally determined by using the standard pair method, observing both a reddened and unreddened star of the same spectral type and comparing their fluxes (e.g. Massa, Savage, & Fitzpatrick 1983; Witt, Bohlin, & Stecher 1984; Fitzpatrick 1990). The attenuation curve of a galaxy is defined as the change in the galaxy's flux due to the presence of dust. This means the attenuation curve is dependent on both the physical properties of the dust grains *and* the spatial distribution of the stars and dust. Thus, the attenuation curve of a galaxy cannot be used directly to probe the composition of the dust grains.

Due to the complexity in studying the dust in the integrated SED of a galaxy, multiwavelength observations covering a long baseline are needed. For the average Milky Way type dust ($R_V = 3.1$), the dust extinction at 1500 Å is 2.5 times the extinction at 5500 Å (V) which is 10 times the extinction at 2.2 μm (K) (Whittet 1992). Therefore, multiwavelength ob-

servations probe a large dynamical range of the dust attenuation and allow one to better constrain the dust spatial distribution and physical properties.

Multiwavelength observations of starbursts, from the UV to the K-band, have recently been used to derive the general behavior of dust attenuation in starburst galaxies (Calzetti, Kinney, & Storchi-Bergmann 1994, 1996; Calzetti 1997). The average attenuation curve for starbursts was determined using a method similar to the standard pair method for determining extinction curves. The starburst SEDs were collected into bins according to their ionized gas $E(B - V)_i$ values (Storchi-Bergmann, Calzetti, & Kinney 1994; Calzetti et al. 1994) and attenuation curves were determined using the smallest $E(B - V)_i$ bin as the unattenuated stellar population. When scaled by their respective $E(B - V)_i$ values, the attenuation curves were roughly similar in shape and strength, and this is the behavior of dust in a screen-like geometry. When normalized to an $E(B - V) = 1$, the resulting average starburst attenuation curve has a slope similar to the MW extinction curve, but lacks a 2175 Å bump, like the SMC extinction curve. Generally, the dust distribution can be described by a distribution of foreground clumps. The strength of the attenuation affecting the stars was found to be different than that affecting the gas, implying that the stars have a dust covering factor smaller (by $\sim 40\%$) than the gas. This implies the stars and gas have different spatial distributions. While the flatter attenuation curve can be explained as an effect of the radiative transfer in the dust, we will argue in this paper the lack of a 2175 Å bump in the average attenuation curve can only be explained by a dust extinction curve with a weak or missing bump.

Without prior knowledge of the dust's type and distribution or stellar evolutionary history in starbursts, the only way to investigate the SED of a starburst is to combine a stellar evolutionary synthesis model with a model for the radiative transfer in dust and simultaneously solve for the characteristics of the stars and dust. The aim of this work is to investigate a large sample of starbursts and derive the geometry and type of dust present in starbursts. In future work, this will allow us to investigate with greater confidence the evolutionary history of individual starbursts. In §2, we discuss our model of a starburst galaxy which includes stellar evolutionary synthesis and the radiative transfer through the starburst's dust. The observational sample (consisting

of 30 starburst galaxy SEDs) used in this paper is described in §3. Section 4 presents color-color plots useful for detecting dust in starbursts as well as constraining the type and spatial distribution of the dust. As an example, we apply our starburst model to the galaxies NGC 4385 & NGC 7714 in §5. We discuss our results and their implications in §6. Finally, our conclusions are presented in §7.

2. Starburst Model

In order to model the SED of starburst galaxies, both a stellar evolutionary synthesis model and a dust radiative transfer model are needed. We combine the stellar evolutionary synthesis models of Leitherer & Heckman (1995; hereafter LH95) and Bruzual & Charlot (1993, 1997; hereafter BC97) to obtain the intrinsic SEDs of both continuous and instantaneous bursts of star formation with ages between 1×10^6 and 15×10^9 years. We use a radiative transfer code based on Monte Carlo techniques to model the effects of dust on the intrinsic SEDs for both MW and SMC type dust.

2.1. Radiative Transfer in Dust

In order to accurately model the radiative transfer of the stellar photons through the dust, we rely on Monte Carlo techniques (Witt 1977). With these techniques, photons are followed through a dust distribution and their interaction with the dust is parameterized by the dust optical depth (τ), albedo, and scattering phase function asymmetry (g). The optical depth determines where the photon interacts, the albedo gives the probability the photon is scattered from a dust grain, and the scattering phase function gives the angle at which the photon scatters. As the physical properties of dust in different environments vary greatly (Witt, Bohlin, & Stecher 1984; Cardelli, Clayton, & Mathis 1989; Fitzpatrick 1989; Mathis & Cardelli 1992), we have chosen to model two extremely different kinds of dust: MW and SMC. For both kinds of dust, we have compiled the wavelength dependence (1200–23,000 Å) of the optical depth, albedo, and g in Table 1. For MW type dust, the τ/τ_V values are from Whittet (1992) and the albedo and g values were determined from smooth curves drawn through many empirical determinations taken from the literature (e.g. Gordon et al. 1994 [and references therein]; Calzetti et al. 1995; Lehtinen & Mattila 1996). For SMC type dust, the τ/τ_V values

are from Prévot et al. (1984) and the albedo and g values were kindly computed for us by Sang-Hee Kim (Kim, Martin, & Hendry 1994; Kim 1996) assuming that the SMC extinction curve is produced by a mixture of silicate and graphite grains. The characteristics of the magnitude bands (UV1 to K) are given in Table 3.

The spatial distribution of the stars and dust was investigated by assuming either dusty or shell geometries. We expect these geometries to bracket the large range of observational star/dust distributions. Following WTC, the dusty geometry has stars and dust uniformly mixed through the entire sphere and the shell geometry (nuclei geometry in WTC) has a dust-free sphere of stars ($r < 0.3r_{\text{max}}$) surrounded by a star-free shell of dust ($0.3r_{\text{max}} < r < r_{\text{max}}$). Unlike WTC, we also allow the dust to be either homogeneous or clumpy (two-phases) on a local scale (but see Witt, Gordon, & Madsen (1997) for an extension of WTC to include clumpy dust). The two-phase clumpy dust is characterized by the ratio of inter-clump to clump medium density (k_2/k_1), the filling factor (ff) of the high density clumps, and the size of the clumps compared to the system size (Witt & Gordon 1996).

The radiative transfer model has the following inputs: the geometry (dusty or shell), homogeneous or clumpy dust distribution (k_2/k_1 , ff, & clump size), radial τ in the V band (equivalent to dust mass), and either MW or SMC type dust grain properties (τ , albedo, and g [see Table 1]). The different model runs are listed in Table 2. All model runs were computed for ff = 0.15 (Witt & Gordon 1996), a clump size of 10% of the system size (radius), and $0.05 \leq \tau_V \leq 40$.

2.2. Stellar Evolutionary Synthesis

The description of the stellar evolution of the starbursts is derived from the work of LH95 and BC97.

LH95 concentrated on the stellar evolutionary synthesis of massive stars, including nebular emission associated with massive stars. They produce SEDs for the two different extreme cases of star formation, instantaneous and constant. For both cases of star formation, we use an initial mass function (IMF) with a Salpeter (1955) slope ($\alpha = 2.35$), a mass range of 1–100 M_{\odot} , and solar metallicity. We have adjusted the absolute level of the SEDs to reflect a mass range of 0.1–100 M_{\odot} using equation 3 in LH95. Since their model lacks information about the later stages of stel-

lar evolution, we limit our use of their SEDs to those with ages less than 2×10^7 years.

BC97 present a stellar evolutionary synthesis code which produces SEDs for both instantaneous and constant star formation. The SEDs are formed using an IMF with a Salpeter (1955) slope ($\alpha = 2.35$), a mass range of 0.1–125 M_{\odot} , and solar metallicity. As this code lacks information on the nebular continuum, we limit our use of these SEDs to the ages between 5×10^7 and 1.5×10^{10} years. In the continuous star formation case, where the nebular contribution from the most recent generation of stars is present, we add the nebular continuum calculated from a LH95 model of constant star formation for an age of 2×10^7 years.

While both LH95 and BC97 provide SEDs computed for metallicities other than solar, we have chosen to use only the solar metallicity SEDs for three reasons. First, the average metallicity of the observed starbursts is relatively high, around 0.5 solar (see §3). Second, theoretical models of low metallicity stellar populations still have difficulties in reproducing all the observational constraints (e.g., the ratio of blue/red supergiants, see Maeder & Conti [1994]). Third, using model SEDs with a higher metallicity than actually observed will result in a lower limit on the effects of dust. This is due to the fact that the lower the metallicity the bluer the SED (Worthey 1994) and since effects of dust are to redden the SED, using solar metallicity SEDs will give a lower limit on the dust’s effects. In future work, we will use SEDs of the observed metallicities when investigating the stellar evolutionary history of individual starbursts.

The upper mass limit on the IMF between the two models is different; 100 M_{\odot} for LH95 and 125 M_{\odot} for BC97. This is not expected to be important as the IMF is steep, the amount of mass between 100 and 125 M_{\odot} is less than 1% of the total mass, and its relative contribution to the ionization and heating of the interstellar medium is small.

Using the above stellar evolutionary models, SEDs from 1000–23,000 Å were generated with ages between 1×10^6 and 15×10^9 years. These SEDs were convolved with photometric bandpasses at UV, optical, and IR wavelengths to generate the intrinsic colors of the starburst model galaxies. In the UV, 7 square bandpasses (UV1–UV7) were defined with standard UV zero magnitude fluxes (Wesseliuss et al. 1982). For the optical and IR, photometric bandpasses for UB-VRIJHK were taken from Bessell & Brett (1988) and Bessell (1990). The zero magnitude fluxes for the UB-

TABLE 1
DUST PHYSICAL PROPERTIES

band	τ/τ_V	MW		τ/τ_V	SMC	
		albedo	g		albedo	g
UV1	3.11	0.60	0.75	5.00	0.40	0.53
UV2	2.63	0.67	0.75	4.36	0.40	0.53
UV3	2.50	0.65	0.73	3.51	0.58	0.54
UV4	2.78	0.55	0.72	3.20	0.58	0.51
UV5	3.12	0.46	0.71	2.90	0.55	0.46
UV6	2.35	0.56	0.70	2.40	0.56	0.37
UV7	2.00	0.61	0.69	2.13	0.53	0.35
U	1.52	0.63	0.65	1.58	0.46	0.34
B	1.32	0.61	0.63	1.35	0.43	0.32
V	1.00	0.59	0.61	1.00	0.43	0.29
R	0.76	0.57	0.57	0.74	0.41	0.26
I	0.48	0.55	0.53	0.52	0.38	0.23
J	0.28	0.53	0.47	0.28	0.33	0.21
H	0.167	0.51	0.45	0.17	0.30	0.23
K	0.095	0.50	0.43	0.11	0.29	0.22

TABLE 2
MODEL RUN INPUTS

run	geometry	k_2/k_1	dust type
1	shell	1.0	MW
2	shell	0.1	MW
3	shell	0.01	MW
4	shell	0.001	MW
5	shell	1.0	SMC
6	shell	0.1	SMC
7	shell	0.01	SMC
8	shell	0.001	SMC
9	dusty	1.0	MW
10	dusty	0.1	MW
11	dusty	0.01	MW
12	dusty	0.001	MW
13	dusty	1.0	SMC
14	dusty	0.1	SMC
15	dusty	0.01	SMC
16	dusty	0.001	SMC

VRI bands were calculated by convolving the appropriate bandpass with the observed spectrum of Vega (Tüg, White, & Lockwood 1977). The calibrated spectrum of Vega was multiplied by 1.028 before use to account for the fact that Vega’s V magnitude is 0.03 (Hoffleit & Warren 1991). The zero magnitude fluxes for the JHK bands were taken from (Bessell 1990). The λ_{eq} , $\Delta\lambda$, and zero magnitude fluxes for the adopted bandpasses are presented in Table 3.

3. Observations

For this paper, we use a sample of 30 starburst galaxies which have SEDs available in the literature. For consistency, we provide a brief summary of the characteristics of galaxies and the properties of the SEDs. We refer the reader to the original papers for the observational details (Kinney et al. 1993; Mcquade, Calzetti, & Kinney 1995; Storchi-Bergmann, Kinney, & Challis 1995; Calzetti 1997).

The galaxies are from the *IUE* Atlas of Kinney et al. (1993) and are characterized by the presence of active star formation in their central regions. The star formation activity manifests itself as strong UV SEDs and intense line emission at optical and IR wavelengths. The galaxies are nearby (median distance 60 Mpc for $H_0 = 50 \text{ km s}^{-1} \text{ Mpc}^{-1}$) irregulars or spirals with disturbed morphologies. The metallicity of the starbursts’ ionized gas is in the range 0.1–2 solar, with a median around 0.5 solar.

Aperture-matched UV and optical SEDs (Kinney et al. 1993; Mcquade, Calzetti, & Kinney 1995; Storchi-Bergmann, Kinney, & Challis 1995) are available for all 30 galaxies and aperture-matched IR photometry at J, H, and K (Calzetti 1997) is available for 19 of the galaxies. The *IUE* aquired UV portion of the SED was corrected to reflect the newest *IUE* absolute calibration (Bohlin 1996). The match in observational apertures ensured that the same region was sampled within each galaxy. Since the UV SEDs were acquired with *IUE*, apertures of $10'' \times 20''$ were used for the optical and IR observations. Differences in orientation between the IUE and optical apertures produced an estimated 10–20% flux mismatch between the two wavelength regions. This size aperture subtends large regions within each galaxy, a diameter of ~ 4.5 kpc at the median distance of 60 Mpc.

In most cases, the UV and optical SEDs cover the wavelength range 1250–7500 Å continuously with a resolution 6 Å in the UV and ~ 10 Å in the optical.

The availability of spectral information allowed us to assess the importance of the emission line contribution to the broad band photometry. The IR images (Calzetti 1997) were used to obtain the J, H, and K photometry with in an area of $10'' \times 20''$ in the E–W direction. In the IR, the contribution of the emission lines to the broad band photometry is negligible, except for the J-band photometry of NGC 4861, where the hydrogen recombination line $\text{Pa}\beta$ (12818 Å) contributes 9% of the band flux (Calzetti 1997).

As with the SEDs produced with the stellar evolutionary models, the SEDs of the 30 starbursts were convolved with photometric bandpasses at UV and optical wavelengths to determine their UV2–I photometry. Prior to this, the SEDs were corrected for foreground Galactic extinction, shifted to zero redshift, and cleaned of emission lines. The dereddening was done using the average Galactic extinction curve (Whittet 1992) and the values of $E(B - V)_G$ listed in Table 1 of Calzetti, Kinney, & Storchi-Bergmann (1994). The SEDs were shifted to zero redshift using the values of z listed in the same table. The emission lines were removed as the stellar evolutionary synthesis model SEDs did not include emission lines and we wish to compare the observations to these models. The IR photometry was transformed from the CIT system (Elias et al. 1982) to the homogeneous system defined by the equations in Bessel & Brett (1988). The resulting magnitudes from the UV, optical, and IR are tabulated in Table 4. The uncertainties in the tabulated magnitudes are 0.10 for UV2–UV7 (Bohlin et al. 1990; Bohlin 1997), 0.10–0.20 for U–I (0.10 for those galaxies with both UV7 and U data), and 0.09–0.14 for J–K (Kinney et al. 1993; Mcquade, Calzetti, & Kinney 1995; Storchi-Bergmann, Kinney, & Challis 1995; Calzetti 1997). Due to mismatches between the apertures used in obtaining the optical and IR photometry, the relative uncertainties between these two wavelength regions are 0.10–0.20 magnitudes. In all the plots in this paper, we have assumed a uncertainty of 0.10 for UV2–UV7 data, 0.10 for U–I for galaxies with UV7 and U data, 0.15 for U–I for galaxies without both UV7 and U, and 0.125 for J–K. For colors involving only J–K, we have used a uncertainty of 0.07 for (J–H) and 0.05 for (H–K) (Calzetti 1997).

4. Color-Color Plots

The main problem with accurately modeling the ages of the stellar populations and effects of dust in a

TABLE 3
MAGNITUDE BAND DEFINITIONS

band	λ_{eq} [Å]	$\Delta\lambda$ [Å]	F_{λ}^{a} [ergs cm ⁻² s ⁻¹ Å ⁻¹]
UV1	1250	250	3.63×10^{-9}
UV2	1515	280	3.63×10^{-9}
UV3	1775	260	3.63×10^{-9}
UV4	1995	200	3.63×10^{-9}
UV5	2215	260	3.63×10^{-9}
UV6	2480	290	3.63×10^{-9}
UV7	2895	560	3.63×10^{-9}
U	3605	640	3.41×10^{-9}
B	4413	959	6.60×10^{-9}
V	5512	893	3.70×10^{-9}
R	6594	1591	2.35×10^{-9}
I	8059	1495	1.15×10^{-9}
J	12369	2034	3.12×10^{-10}
H	16464	2862	1.14×10^{-10}
K	21578	2673	3.94×10^{-11}

^a F_{λ} is the flux corresponding to a magnitude of zero. See text for details.

TABLE 4
STARBURST GALAXY PHOTOMETRY

name	UV2	UV3	UV4	UV5	UV6	UV7	U	B	V	R	I	J	H	K
IC 1586	14.27	14.34	14.77	15.32	14.92	13.58	12.83	12.52
HARO 15	12.99	13.14	14.37	15.02	14.78	14.53	14.05	13.54	12.92	12.58
MRK 357	13.29	13.55	14.90	15.87	15.79	14.55	13.86	13.39
IC 214	14.10	14.14	15.59	16.03	15.48	12.66	11.85	11.37
NGC 1140	11.96	12.17	13.11	13.75	13.43	13.18	12.74	12.54	11.86	11.62
NGC 1510	12.91	13.14	13.42	13.56	13.87	14.02	14.33	14.87	14.55	14.25
NGC 1569	9.68	9.72	9.95	10.18	10.19	10.46	10.71	11.66	11.47	11.36	...	10.93	10.29	10.12
NGC 1614	14.16	14.16	14.18	14.57	13.91	13.36	12.57	11.46	10.60	10.07
NGC 1705	10.55	10.94	11.23	11.40	11.82	12.27	12.70	13.61	13.43	13.22	12.79
NGC 3049	13.54	13.58	13.80	13.92	14.08	14.22	14.44	15.09	14.64	14.30	13.82
NGC 3125	12.24	12.33	12.68	12.85	13.10	13.34	13.50	14.32	14.08	13.73	13.24
NGC 4194	13.39	13.31	13.44	13.52	13.57	13.48	13.40	13.96	13.35	11.43	10.67	10.24
NGC 4385	13.30	13.29	13.55	13.53	13.87	13.98	14.17	14.71	14.09	13.47	12.82	12.14	11.44	11.12
NGC 4861	11.43	11.78	12.17	12.54	12.77	13.07	14.91	14.89	...	13.83	13.41	13.10
NGC 5236	10.32	10.30	10.43	10.48	10.70	10.83	11.02	11.60	11.13	10.80	10.23
NGC 5253	10.61	10.75	10.91	11.07	11.35	11.65	12.05	12.93	12.75	12.53	12.24
UGC 9560	12.69	12.98	13.32	13.54	13.76	14.13	14.65	15.59	15.32	15.13
NGC 5860	14.23	14.19	14.71	14.76	14.79	14.66	14.57	14.91	14.34	12.87	12.12	11.83
NGC 5996	13.36	13.37	13.67	13.56	13.84	13.97	14.10	14.74	14.28
NGC 6052	13.36	13.36	13.59	13.72	13.84	13.96	13.81	14.42	14.03	13.91	...	12.77	12.13	11.82
NGC 6090	13.86	13.82	14.58	15.14	14.64	14.31	...	12.65	11.92	11.46
NGC 6217	13.04	12.93	14.11	13.55	13.15	...	11.55	10.80	10.45
TOL 1924-416	11.90	12.19	12.50	12.73	13.03	13.33	13.49	14.27	13.95	13.74	13.45
NGC 7250	12.42	12.51	12.80	12.69	13.06	...	13.69	14.48	14.17	13.94	...	13.00	12.39	12.12
NGC 7552	13.34	13.06	13.12	13.03	13.02	12.94	12.65	12.99	12.38	11.90	11.17
NGC 7673	12.72	12.85	13.12	13.31	13.53	13.69	13.61	14.19	13.82	13.60	...	12.63	12.02	11.73
NGC 7714	12.18	12.27	12.56	12.71	12.84	12.95	13.11	13.81	13.43	13.07	12.59	11.87	11.17	10.81
NGC 7793	13.64	13.77	14.02	14.27	14.44	14.40	14.22	14.60	13.99	13.58	12.97
MRK 309	14.92	14.79	15.13	15.81	15.43	13.77	13.05	12.54
MRK 542	14.21	14.37	15.51	15.80	15.27	13.66	13.01	12.66

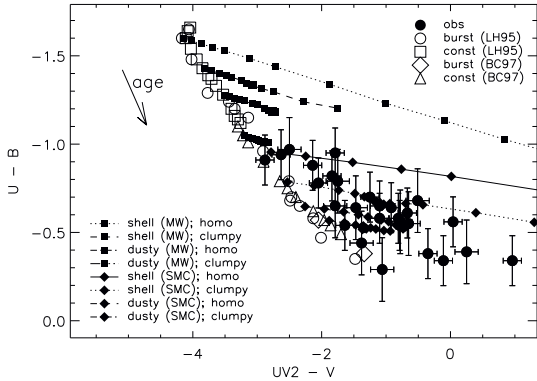


Fig. 1.— The color-color plane (U-B) vs. (UV2-V) is plotted for both the starburst observations and models. The dust reddening trajectories can start from any stellar evolutionary synthesis model, but to plot them, they were attached to an arbitrary stellar evolutionary synthesis model. The clumpy geometry refers to a $k_2/k_1 = 0.01$. The words burst and const in the upper legend refer to the kind of star formation (instantaneous or constant, respectively) assumed in the stellar evolutionary synthesis models. The age vector points in the direction of increasing age of the stellar evolutionary synthesis SEDs.

galaxy is that aging the stellar population and adding dust both redden the galaxy’s SED. A non-exhaustive search of the *many* color-color plots turned up a handful of plots where the effects of stellar population changes were in a different direction in the color-color plane than those due to the dust. By examining where the sample of observed starburst galaxies fall on these color-color plots, information about the dust (type/geometry) and the stellar population (burst/constant and age) can be derived.

The color-color plot (U-B) vs. (UV2-V) is plotted in Figure 1 and plainly shows the presence of dust in starburst galaxies. All of the stellar evolutionary synthesis models fall in a well defined line, with age increasing downward, while the actual observations all lie to the right of this line. Combining different stellar evolutionary models to approximate a starburst with a complex stellar evolutionary history will not move the starburst off of the line defined by the simple stellar evolutionary models. All of the reddening trajectories point to the right but some are not long

enough to explain the spread in the observed starbursts. Those which cannot explain the spread are the dusty geometry models which assume the same global distributions of stars and dust, be they homogeneous or clumpy. The shell geometry can explain the observed spread and we adopt this as the geometry for starburst galaxies. This geometry results in a screen-like behavior of the dust which allowed Calzetti et al. (1994) to derive an average attenuation curve for starbursts in a manner analogous to the standard pair method. It is important to remember that an attenuation curve is an extinction curve convolved with the dust geometry and thus an attenuation curve cannot be used to probe the type of dust grains directly.

From Figure 1, the stellar population can be constrained by moving along the reddening trajectories back to the line defined by the stellar evolutionary models. The stellar populations seem to arise from burst star formation models with ages between 8×10^6 and 2×10^8 years or constant star formation models between 1×10^8 and 15×10^9 years. Actually determining the star formation history of an individual galaxy is quite complex and requires fitting the SED from the UV to the IR. See §5 for an example of how this can be done. The absence of starbursts (from our UV selected sample) with ages $< 8 \times 10^6$ years suggests the initial phase of starbursts is hidden within dust clouds and is difficult to observe in the UV. In addition, the age we derive is the average age of the starburst regions falling in the large aperture used to obtain the SEDs. Thus, starburst regions with ages $< 8 \times 10^6$ years could be present, but washed out by the presence of older starburst regions.

Figures 2–4 show examples of useful color-color plots (one each for the UV, optical, and IR) which show differences between stellar population changes and dust reddening. The (UV2-UV3) vs. (UV2-UV7) color-color plane (Figure 2) is a good plane in which to investigate whether SMC or MW type dust best matches the type of dust in starbursts. The observations fall between the SMC and MW reddening trajectories, but closest to the SMC reddening trajectories. This implies the far-UV slope of the starbursts’ extinction curve has a value between the MW and SMC, but closest to the SMC. In §4.1, we investigate the starbursts’ UV extinction curve in more detail, focusing on the 2175 Å bump. The optical (U-B) vs. (B-V) color-color plane (Figure 3) does show that dust is present, but the effects are not as definitive as those shown in the previous two figures. This points

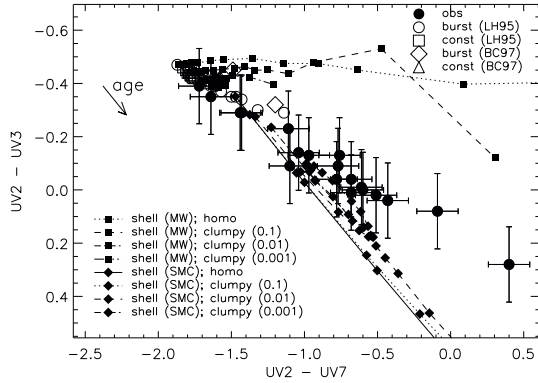


Fig. 2.— The color-color plane (UV2-UV3) vs. (UV2-UV7) is plotted. The number in parenthesis after the word clumpy in the lower legend refers to the value of k_2/k_1 . Otherwise, this figure was constructed in a manner similar to Figure 1.

to the need, in investigating the dust in starbursts, for SEDs covering more than just the optical. The (J-H) vs. (H-K) color-color plane (Figure 4) also shows the effects of dust, but some degeneracy exists between changes in age and the effects of dust. In addition, not all of the starbursts can be traced back to a stellar population model through the reddening trajectories. This is probably due to problems with stellar evolutionary models in the IR region (see LH95 and Lançon & Rocca-Volmerange [1996] for details). While all of the above color-color plots (Figures 1–4) clearly show the presence of dust in starbursts, the diagnostic utility of color-color plots is greatest in the UV.

4.1. Absence of the 2175 Å bump

Due to its prominence, the 2175 Å extinction bump is an excellent probe of the type of dust in a galaxy. This is illustrated by the average extinction curves of the MW, LMC, SMC, and M31, all of which show different 2175 Å strengths (Fitzpatrick 1989; Bianchi et al. 1996). The lack of a depression at 2175 Å in SEDs of starbursts has raised the question: does the dust in starbursts lack a 2175 Å bump or are there radiative transfer effects associated with the spatial distribution of the dust which weaken the bump below observational detection? To investigate this question, two color-color plots were constructed. Figures 5 & 6 show the (UV4-UV5) vs. (UV4-UV6) and (U-B)

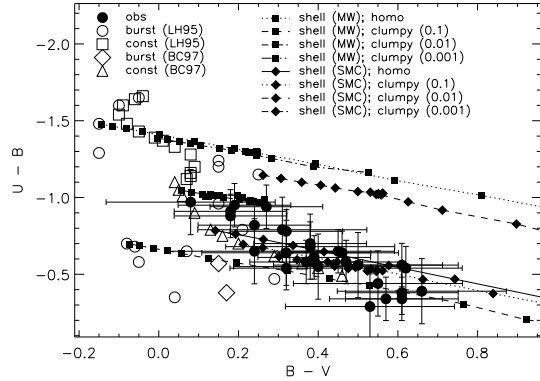


Fig. 3.— The color-color plane (U-B) vs. (B-V) is plotted. The number in parenthesis after the word clumpy in the right legend refers to the value of k_2/k_1 . Otherwise, this figure was constructed in a manner similar to Figure 1.

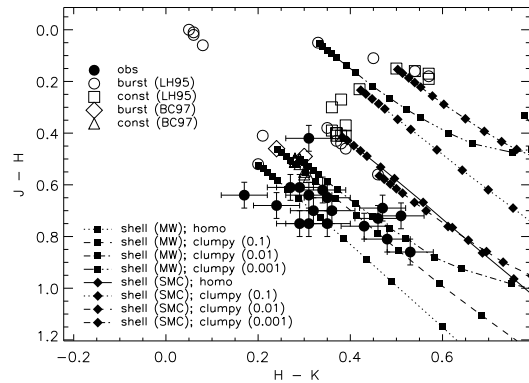


Fig. 4.— The color-color plane (J-H) vs. (H-K) is plotted. The number in parenthesis after the word clumpy in the lower legend refers to the value of k_2/k_1 . Otherwise, this figure was constructed in a manner similar to Figure 1.

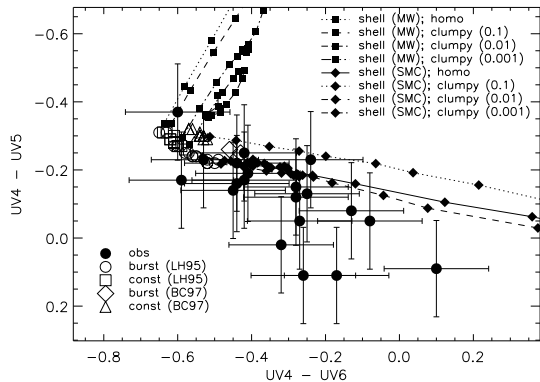


Fig. 5.— The color-color plane (UV4-UV5) vs. (UV4-UV6) is plotted. The number in parenthesis after the word clumpy in the lower legend refers to the value of k_2/k_1 . Otherwise, this figure was constructed in a manner similar to Figure 1.

vs. (UV4-UV5) color planes, respectively. The placement of the three bandpasses of UV4, UV5, & UV6 ($\lambda_{\text{eq}} = 1995 \text{ \AA}$, 2215 \AA , & 2480 \AA) make them ideal for studying the 2175 \AA bump. The color (UV4-UV6) measures the slope underneath the 2175 \AA bump and the color (UV4-UV5) is sensitive to the short wavelength slope of the 2175 \AA bump.

Both figures clearly show the SMC reddening trajectories generally point toward the starburst observations, while the MW reddening trajectories completely miss the observations. In Figure 5 the MW reddening trajectories point almost 90° from the observations and in Figure 6 they point almost 180° from the observed starbursts. One of the MW reddening trajectories shows how radiative transfer effects can reduce the strength of the 2175 \AA bump. In Figure 5, the reddening trajectory for model run 4 (shell, MW clumpy with $k_2/k_1 = 0.001$) loops back toward the stellar evolutionary models. This is caused by the output spectrum being dominated by unattenuated stars which suppress both the 2175 \AA bump as well as the slope of the attenuation curve in the UV. While the starbursts do not show the presence of the 2175 \AA bump, they do show the signature of a substantial UV slope in their attenuation curves. Therefore, radiative transfer effects alone cannot explain the lack of a 2175 \AA bump in starbursts and, so, the dust in the average starburst is more like the

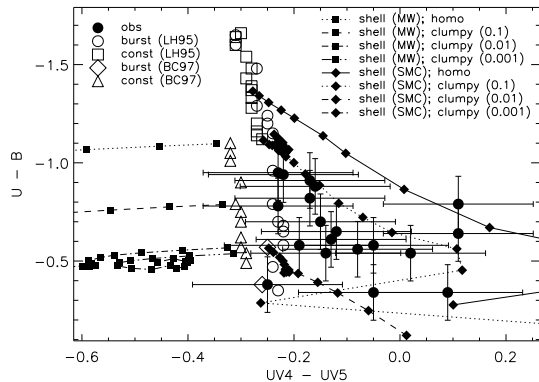


Fig. 6.— The color-color plane (U-B) vs. (UV4-UV5) is plotted. The number in parenthesis after the word clumpy in the lower legend refers to the value of k_2/k_1 . Otherwise, this figure was constructed in a manner similar to Figure 1.

dust in the SMC than in the MW. This agrees with the notion that the dust in starbursts would be similar to the weak 2175 \AA bump 30 Dor region dust, the mini-starburst next door (Walborn 1991).

In Figure 5, there are a number of starbursts which cannot be traced back to the stellar evolutionary models through a reddening trajectory. This is not surprising as we have only investigated two extinction curves and the extinction curves of dust in the MW, LMC, and SMC are known to possess large variations (Lequeux et al. 1982; Prévot et al. 1984; Witt, Bohlin, & Stecher 1984; Fitzpatrick 1985; Cardelli, Clayton, & Mathis 1989). In order to fit these outlying starbursts, we would need an extinction curve in which the color excess in (UV4-UV5) is greater for a given color excess in (UV4-UV6) than that in the SMC extinction curve. This implies an extinction curve with a curvature between UV4 and UV6 greater than curvature in the same region in the SMC extinction curve. Confirmation of this speculation awaits future work where we plan to individually fit each of the starbursts and derive the average starburst extinction curve.

5. NGC 4385 & NGC 7714

Fitting an individual galaxy's SED is difficult as there are usually many starburst models (combina-

tions of stellar evolutionary synthesis and radiative transfer in dust) which can produce the same SED. As an example of this degeneracy, we fit the two galaxies NGC 4385 and NGC 7714 for which we have complete SEDs from UV2 to K. To test the goodness of the fit for a specific starburst model, we used the $\tilde{\chi}^2$ (reduced χ^2) criterion after first normalizing the observed and model SEDs at the K band. The $\tilde{\chi}^2$ was computed using

$$\tilde{\chi}^2 = \frac{1}{d} \sum_{i=1}^n \left(\frac{F_o(\lambda_i) - F_m(\lambda_i)}{\sigma(\lambda_i)} \right)^2 \quad (1)$$

where n is the number of points in the observed SED, d is the number of degrees of freedom, $F_o(\lambda_i)$ is the observed flux at the i th point in the SED, $F_m(\lambda_i)$ is the same for the model flux, and $\sigma(\lambda_i)$ is the i th uncertainty in the observed flux (Taylor 1982). The number of degrees of freedom $d = (n - 1)$ as both the observed and model SEDs were normalized at the K band. Starburst models with $\tilde{\chi}^2 > 1.8$ were rejected as the probability of such models agreeing with the observations was small. With this limiting value of $\tilde{\chi}^2$, we will collect 96.3% of the starburst models which fit the observed SED within the uncertainties (Taylor 1982). Such fits were obtained for 17 and 46 different starburst models for NGC 4385 and NGC 7714, respectively.

The parameters of the starburst models which fit are interesting. Only models containing dust with a SMC extinction curve fit the data, consistent with our findings in §4.1. Using our results from §4 and restricting the fits to models with a shell geometry, the number of starburst models which fit are 8 for NGC 4385 and 18 for NGC 7714. In order to choose among the starburst models which fit the observed SEDs, more information about each starburst (e.g. the number of ionizing photons) must be used and we plan to do this in a future paper. The best fit starburst model for NGC 4385 ($\tilde{\chi}^2 = 1.11$) was for a constant star formation BC97 model with an age of 7×10^9 years, a shell geometry with $\tau_V = 0.75$, and clumpy ($k_2/k_1 = 0.001$) SMC type dust. This best fit starburst model, along with the observed SED of NGC 4385 is displayed in Figure 7a. The best fit starburst model for NGC 7714 ($\tilde{\chi}^2 = 0.49$) was for a constant star formation BC97 model with an age of 1×10^9 years, a shell geometry with $\tau_V = 1.00$, and clumpy ($k_2/k_1 = 0.001$) SMC type dust. This best fit starburst model, along with the observed SED of NGC 7714 is displayed in Figure 7b.

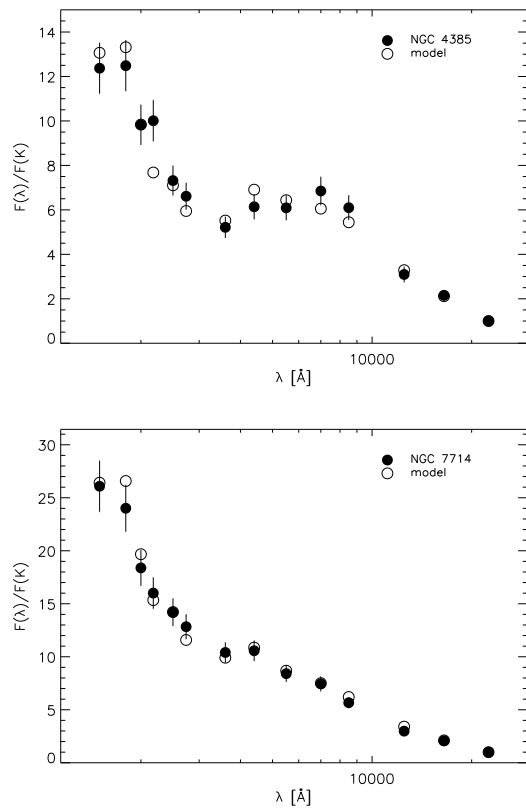


Fig. 7.— The best fit starburst model for NGC 4385 (a, left) and NGC 7714 (b, right) are plotted along with their observed SEDs.

To illustrate the difference between extinction and attenuation curves, Figure 8 displays the SMC extinction curve and the average starburst attenuation curve (Calzetti et al. 1994) with the attenuation curves from the best fit starburst models for NGC 4385 and NGC 7714. For both galaxies, the attenuation curves are flatter than the dust extinction curve and this is consistent with the Calzetti et al. (1994) attenuation curve. Also, the shape of the attenuation curve is different between NGC 4385 & NGC 7714 even though both curves are for a shell geometry with a clumpy ($k_2/k_1 = 0.001$) distribution of SMC dust. This neatly shows the dependence of the shape of an attenuation curve on both the geometry and amount of dust. The systematic difference between the shape of both the NGC 4385 and NGC 7714 attenuation curves and the Calzetti et al. (1994) attenuation curve is likely due to differences between the actual dust albedo and the adopted albedo (Table 1).

Calzetti et al. (1994) determined the effective B band optical depth ($\tau_{B,\text{eff}}$) to be 0.62 for NGC 4385 and 0.42 for NGC 7714. These values of $\tau_{B,\text{eff}}$ were determined from observations of H α and H β ; therefore they measure the $\tau_{B,\text{eff}}$ of the starburst’s gas. The starburst models in this paper measure the starburst’s stars and from the best fit models the $\tau_{B,\text{eff}}$ was 0.26 for NGC 4385 and 0.33 for NGC 7714. This result agrees with the finding by Calzetti (1997) that the gas in starbursts shows a larger dust attenuation than the stars. The gas is likely associated with O stars (H II regions), while the stellar continuum has contributions from a wide range of stars. As O stars are short lived, on average they will be more deeply embedded in their birth clouds and thus the gas will show a larger dust attenuation than the stellar continuum.

6. Discussion

The discovery that the dust in starbursts is closer to SMC type dust than MW type dust is not totally unexpected (Calzetti et al. 1994; Mas-Hesse & Kunth 1996). It has been known that the attenuation curve of starbursts is flat and does not show the presence of the 2175 Å bump, but as a result of this work it is clear this is due to SMC-like dust grains and not radiative transfer effects. The 30 Dor region of the LMC forshadows this conclusion as the dust associated with the massive star formation in the 30 Dor

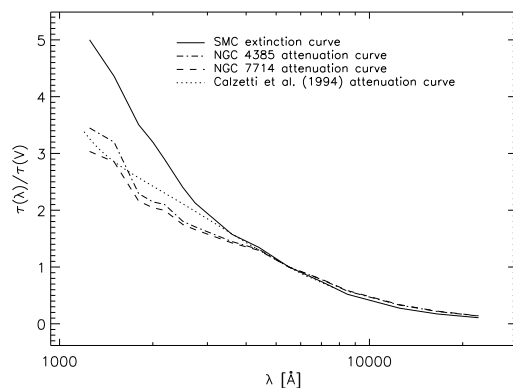


Fig. 8.— This plot shows a comparison of the SMC extinction curve and the Calzetti et al. (1994) average starburst attenuation curve with the attenuations curves from the best fit starburst models of NGC 4385 and NGC 7714. The average starburst attenuation curve was created by normalizing the Calzetti et al. (1994) starburst attenuation curve to the stellar continuum ($E(B-V) = 1$) and adding $R_V = 3.1$. The curves are normalized to the V band. The effective τ_V for NGC 4385 was 0.19 and the input τ_V was 0.75. The effective τ_V for NGC 7714 was 0.25 and the input τ_V was 1.00. The effective τ_V is defined as the τ_V an overlaying screen would need to produce the same reduction in flux.

region is very different than the dust associated with the rest of the LMC. The 30 Dor region dust has a weaker 2175 Å bump and stronger far-UV rise than the dust in the rest of the LMC. Like the 30 Dor region, it is unlikely the dust in starbursts formed with a weak or negligible 2175 Å bump and strong far-UV rise. It is more likely that the dust in starbursts has been modified by the starburst activity to more SMC-like in nature. Again, the 30 Dor region has shown its identity as the Rosetta Stone for starburst galaxies (Walborn 1991).

With this conclusion in hand the question arises: How does starburst activity modify dust such that it loses its 2175 Å bump and strengthens its far-UV rise? The answer lies in the different grain populations which taken together explain dust extinction curves. Dust grains are thought to be composed of three different populations: classically sized grains which produce the optical-IR extinction, small grains which produce the 2175 Å bump, and small grains which produce the far-UV extinction rise (Mathis 1996; Zubko, Krelowski, Wegner 1996; Li & Greenberg 1997). The SMC-like extinction curve in starbursts implies the 2175 Å bump grains are destroyed and the number of far-UV rise grains have been increased. The 30 Dor region has less intense star formation leading to a similar but a notably different extinction curve. This extinction curve implies that the 2175 Å bump grains are still present, but in reduced numbers, and the far-UV rise grains have increased their numbers. Finally, the Orion region has a low level of star formation ($\sim 1\%$ that of 30 Dor [Hunter et al. 1995]) which has also affected the dust's extinction curve. The Orion region extinction curve has a reduced 2175 Å bump and a nearly *flat* far-UV rise (Cardelli & Clayton 1988). This implies both the 2175 Å bump and far-UV rise grains have been reduced in number.

There seems to be a trend in the dust extinction curve with star formation activity. This can be explained by the relative importance of shocks and stellar radiation in the modification of dust grains. In the Orion region, the stellar radiation pressure and evaporation of dust grains have selectively removed the small grains (McCall 1981; Cardelli & Clayton 1988). In starbursts, the dust modification is most likely dominated by supernovae shocks which are efficient at shattering large grains, thus increasing the small grain population (Jones, Tielens, & Hollenbach 1996). This explains the increase in the number of

far-UV rise grains, but the absence of the 2175 Å bump grains implies they do not survive the shocks and are either vaporized or shattered. The 30 Dor region lies between the Orion region and starburst galaxies in star formation activity and, thus, has an extinction curve intermediate between the two. The trend with star formation activity implies the material which makes up the 2175 Å bump grains is not as robust as the material which makes up the far-UV rise grains. The identity of material which gives rise to the far-UV rise and, especially, the 2175 Å bump has remained elusive for many years. For this reason, we do not attempt to discuss the material which produces the 2175 Å bump, but only to note that the trend with star formation activity of the far-UV rise and 2175 Å dust grains is a clue to the identity of the material making those dust grains.

The similarity of the average extinction curves of starbursts and the SMC deserves comment. The lack of a 2175 Å bump and the steep far-UV rise in the SMC extinction curve is attributed to the SMC's low metallicity (Prévot et al. 1984; Clayton & Martin 1985; Fitzpatrick 1986). Since our sample of starbursts possess a large range of metallicities, 0.1–2 solar (see section 3), this is unlikely to explain the SMC-like extinction curve we found in starbursts. We suggest the SMC-like extinction curve in starbursts is a result of the massive star formation. Thus, both metallicity and star formation activity may influence dust properties significantly.

Observations which resolve starburst galaxies show that the star formation occurs in localized regions analogous to the star clusters and associations of our galaxy (O'Connell, Gallagher, & Hunter 1994; O'Connell et al. 1995; Whitmore & Schweizer 1995; Vacca 1996). Not all starbursts seem to form stars this way, see Smith et al. (1996) for an example of a global starburst. These observations allow us to interpret the fact that we were able to model the effects of dust in starbursts with a radiative transfer model with a clumpy shell geometry. The τ_V determined from our starburst model is interpreted as the flux weighted average τ_V to many individual star clusters. From this, it is not surprising we find fairly low τ_V 's as star clusters possessing a large τ_V would not contribute much to the starburst SED. The shell geometry is a realistic approximation of the geometry of the individual star clusters. Near the center of the star clusters where the radiation field is intense, dust grains would be unable to survive and, thus, the inner

region would be fairly free of dust.

We were able to fit the SEDs of NGC 4385 & NGC 7714 by using the same radiative transfer model and only varying the amount of dust. This particular model run (#8, Table 2) had SMC dust, a shell geometry, a clumpy dust distribution with $k_2/k_1 = 0.001$. This gives hope that it will be possible to investigate the stellar evolutionary history of individual starbursts as well as the type and amount of dust present. These fits were done using only the broad band SED of the starbursts and a proper fit would use the full SED. We plan to fit the full SED and fit both the continuum and spectral lines in future work where we plan to investigate each starburst individually.

7. Conclusions

From the comparison of 30 starburst SEDs with a model for starbursts which included both stars and effects of dust, we concluded the following:

1. The dust in starbursts has an extinction curve similar to that found in the SMC, i.e. lacking a 2175 Å bump and having a far-UV rise with a slope intermediate between the MW and SMC. The dust is unlikely to have been formed with these properties, but to have acquired them as a result of the massive star formation occurring in the starburst.
2. The spatial distribution of stars and dust is best described by a shell geometry. This geometry has an inner dust-free sphere of stars surrounded by a star-free shell of dust.
3. The dust distribution in starbursts is best described by a locally clumpy distribution.
4. The age of the stellar populations in this UV selected sample of starbursts ranges between 8×10^6 and 2×10^8 years if a burst star formation is assumed and 1×10^8 and 15×10^9 years if constant star formation is assumed.
5. The effects of dust on the SED of a starburst are characterized by an attenuation curve which is SMC-like extinction curve convolved with the radiative transfer effects associated with a shell star/dust geometry with a clumpy dust distribution. The wanton use of a SMC extinction curve to correct a starburst's SED is not supported by this work.

We thank Sang-Hee Kim for computing the albedo and g values for the SMC dust for us. The comments of the referee, Geoff Clayton, were appreciated and significantly improved this paper. A major portion of this work was done while K. D. Gordon was at the Space Telescope Science Institute as a Collaborative Visitor of D. Calzetti. The Space Telescope Science Institute is operated by the Association of Universities for Research in Astronomy, Inc., under NASA contract NAS 5-26555. K. D. Gordon and A. N. Witt acknowledge financial support from NASA LTSAP grants NAGW-3168 & NAG5-3367 to The University of Toledo.

REFERENCES

- Bessel, M. S. & Brett, J. M. 1988, *PASP*, 100, 1134
- Bessel, M. S. 1990, *PASP*, 102, 1181
- Bianchi, L., Clayton, G. C., Bohlin, R. C., Hutchings, J. B., & Massey, P. 1996, *ApJ*, 471, 203
- Bohlin, R. C., Harris, A. W., Holm, A. V., Gry, C. 1990, *ApJS*, 73, 413
- Bohlin, R. C. 1996, *AJ*, 111, 1743
- Bohlin, R. C. 1997, private communication
- Bruzual, A. G. & Charlot, S. 1993, *ApJ*, 405, 538
- Bruzual, A. G. & Charlot, S. 1997, in preparation [BC97]
- Calzetti, D. 1997, *AJ*, 113, 162
- Calzetti, D., Bohlin, R. C., Gordon, K. D., Witt, A. N., & Bianchi, L. 1995, *ApJ*, 466, L97
- Calzetti, D., Kinney, A. L., & Storchi-Bergmann, T. 1994, *ApJ*, 429, 582
- Calzetti, D., Kinney, A. L., & Storchi-Bergmann, T. 1996, *ApJ*, 458, 132
- Cardelli, J. A. & Clayton, G. C. 1988, *AJ*, 95, 516
- Cardelli, J. A., Clayton, G. C., & Mathis, J. S. 1989, *ApJ*, 345, 245
- Clayton, G. C. & Martin, P. G. 1985, *ApJ*, 288, 558
- Dickey, J. M. & Garwood, R. W. 1989, *ApJ*, 341, 201
- Elias, J. H., Frogel, J. A., Matthews, K., & Neugebauer, G. 1982, *AJ*, 87, 1029

- Fitzpatrick, E. L. 1985, *ApJ*, 299, 219
- Fitzpatrick, E. L. 1986, *AJ*, 92, 1068
- Fitzpatrick, E. L. 1989, in *IAU Symp. 135, Interstellar Dust*, ed. L. J. Allamandola & A. G. G. M. Tielens (Dordrecht: Kluwer), 37
- Fitzpatrick, E. L. & Massa, D. 1990, *ApJS*, 72, 163
- Gordon, K. D., Witt, A. N., Carruthers, G. R., Christensen, S. A., & Dohne, B. C. 1994, *ApJ*, 432, 641
- Hoffleit, D. & Warren, W. H. Jr. 1991, *The Bright Star Catalogue, 5th Revised Ed. (Preliminary Version)*, *Astronomical Data Center*
- Hunter, D. A., Shaya, E. J., Holtzman, J. A., Light, R. M., O'Neil, E. J., & Lynds, R. 1995, *ApJ*, 448, 179
- Jones, A. P., Tielens, G. G. M., & Hollenbach, D. J. 1996, *ApJ*, 469, 740
- Kim, S.-H. 1996, private communication
- Kim, S.-H., Martin, P. G., & Hendry, P. D. 1994, *ApJ*, 422, 164
- Kinney, A. L., Bohlin, R. C., Calzetti, D., Panagia, N., & Wyse, R. F. G. 1993, *ApJS*, 86, 5
- Lançon, A. & Rocca-Volmerange, B. 1996, *New Astronomy*, 1, 215
- Lehtinen, K. & Mattila, K. 1996, *A&A*, 309, 570
- Lequeux, J., Maurice, E., Prévot-Burnichon, M. L., Prévot, L., & Rocca-Volmerange, B. 1982, *A&A*, 113, L15
- Leitherer, C. & Heckman, T. M. 1995, *ApJS*, 96, 9 [LH95]
- Li, A. & Greenberg, J. M. 1997, *A&A*, in press
- Maeder, A. & Conti, P. S. 1994, *ARA&A*, 32, 227
- Mas-Hesse, J. M. & Kunth, D. 1996, in *The Interplay Between Massive Star Formation, The ISM and Galaxy Evolution*, eds. D. Kunth et al. (France: Editions Fronteires), 401
- Massa, D., Savage, B. D., Fitzpatrick, E. L. 1983, *ApJ*, 266, 662
- Mathis, J. S. 1996, *ApJ*, 472, 643
- Mathis, J. S. & Cardelli, J. A. 1992, *ApJ*, 398, 610
- McCall, M. L. 1981, *MNRAS*, 194, 485
- Mcquade, K., Calzetti, D., & Kinney, A. L. 1995, *ApJS*, 97, 331
- O'Connell, R. W., Gallagher, J. S. III, & Hunter, D. A. 1994, *ApJ*, 433, 65
- O'Connell, R. W., Gallagher, J. S. III, Hunter, D. A., & Colley, W. N. 1995, *ApJ*, 446, L1
- Prévot, M. L., Lequeux, J., Maurice, E., Prévot, L., & Rocca-Volmerange, B. 1984, *A&A*, 132, 389
- Rosen A. & Bregman, J. N. 1995, *ApJ*, 440, 634
- Salpeter, E. E. 1955, *ApJ*, 121, 161
- Scalo, J. 1990, in *Physical Processes in Fragmentation & Star Formation*, eds. R. Capuzzo-Dolcetta et al. (Dordrecht: Kluwer)
- Smith, D. A., et al. 1996, *ApJ*, 473, L21
- Storchi-Bergmann, T., Calzetti, D., & Kinney, A. L. 1994, *ApJ*, 429, 572
- Storchi-Bergmann, T., Kinney, A. L., & Challis, P. 1995, *ApJS*, 98, 103
- Taylor, J. R. 1982, *An Introduction to Error Analysis* (Mill Valley, CA: Univ. Science Books)
- Tüg, H., White, N.M., & Lockwood, G.W. 1977, *A&A*, 61, 679
- Vacca, W. D. 1996, in *The Interplay Between Massive Star Formation, The ISM and Galaxy Evolution*, eds. D. Kunth et al. (France: Editions Fronteires), 321
- Walborn, N. R. 1991, in *Massive Stars in Starbursts*, eds. C. Leitherer et al. (Cambridge: Cambridge Univ. Press), 145
- Wesselius, P. R., van Duinen, R. J., de Jonge, A. R., Aalders, J. W. G., Luinge, W., & Wildeman, K. J. 1982, *A&AS*, 49, 427
- Whitmore, B. C. & Schweizer, F. 1995, *AJ*, 109, 960
- Whittet, D. C. B. 1992, *Dust in the Galactic Environment* (Bristol: IOP)
- Witt, A. N. 1977, *ApJS*, 35, 1

Witt, A. N., Bohlin, R. C., & Stecher, T. P. 1984,
ApJ, 279, 698

Witt, A. N. & Gordon, K. D. 1996, ApJ, 463, 681

Witt, A. N., Gordon, K. D., & Madsen, G. M. 1997,
in preparation

Witt, A. N., Thronson, H. A., & Capuano, J. M. 1992,
ApJ, 393, 611 [WTC]

Worthey, G. 1994, ApJS, 95, 107

Zubko, V. G., Krełowski, J., & Wegner, W. 1996,
MNRAS, 283, 577